

# Magnetic properties of spin-orbital polarons in lightly doped cobaltates

M. Daghofer, P. Horsch, and G. Khaliullin

Max-Planck-Institut für Festkörperforschung, Heisenbergstrasse 1, D-70569 Stuttgart, Germany

(Dated: May 12, 2006)

We present a numerical treatment of a spin-orbital polaron model for  $\text{Na}_x\text{CoO}_2$  at small hole concentration ( $0.7 < x < 1$ ). We demonstrate how the polarons account for the peculiar magnetic properties of this layered compound: They explain the large susceptibility; their internal degrees of freedom lead both to a negative Curie-Weiss temperature and yet to a ferromagnetic intra-layer interaction, thereby resolving a puzzling contradiction between these observations. We make specific predictions on the momentum and energy location of excitations resulting from the internal degrees of freedom of the polaron, and discuss their impact on spin-wave damping.

PACS numbers: 71.27.+a, 75.30.Ds, 75.30.Et

The complex physics of transition metal oxides often leads to intriguing and potentially rewarding properties like, e.g., high- $T_C$  superconductivity in the case of cuprates or colossal magnetoresistance in the case of manganites. The layered cobaltate  $\text{Na}_x\text{CoO}_2$  is of interest mainly for two reasons: When it is hydrated, the resulting  $\text{Na}_x\text{CoO}_2 \cdot y\text{H}_2\text{O}$  becomes superconducting for doping  $x \approx 0.3$ ,  $y \approx 1.4$  [1]. Without hydration, it shows an exceptionally high thermopower, i.e. the capability to transform temperature differences into electricity, for  $0.5 \leq x \leq 0.9$  [2, 3] in an unusual combination with low resistivity. Magnetic fields strongly affect the thermopower in this material [4], which suggests that electron-electron correlations and spin degrees of freedom are important. These remarkable features of cobaltates have triggered large interest due to their potential applications, therefore, the origin of the exotic transport and magnetic properties of  $\text{Na}_x\text{CoO}_2$  is one of the hot topics in the field of strongly correlated materials.

While  $\text{Na}_x\text{CoO}_2$  does not show magnetic order either for  $x < 0.7$  (except at  $x = 0.5$ ) [5] or for  $x = 1$  [6], it is found in the  $A$ -type antiferromagnetic phase below  $T_N \approx 20\text{K}$  for  $0.7 < x < 0.9$  [7, 8]. In this phase, the carriers move on a hexagonal lattice within the ferromagnetic planes, which are antiferromagnetically stacked. The lattice spacing within the planes is much smaller than between them which typically leads to considerably stronger in-plane coupling in such layered systems, e.g. in  $\text{NaNiO}_2$  with the same crystal structure [9]. Surprisingly, this is not the case here: The ferromagnetic in-plane coupling is only of the order of magnitude of the antiferromagnetic inter-layer coupling [7] or even smaller [8]. At higher temperatures  $T \gg T_N$ , the susceptibility  $\chi$  shows Curie-Weiss behavior, i.e.  $\chi \propto 1/(T - \theta)$ , with a *negative* Curie-Weiss temperature  $\theta < 0$  [3, 4, 10, 11, 12]. As has been pointed out in Ref. 7, this contradicts the *positive* Curie-Weiss temperature inferred from spin-wave data.

In this letter, we analyze a spin-orbital polaron model proposed in Ref. 13 for  $\text{Na}_x\text{CoO}_2$  at large  $x$  (i.e. small hole concentration). By means of unbiased numerical techniques, we calculate static and dynamic observables

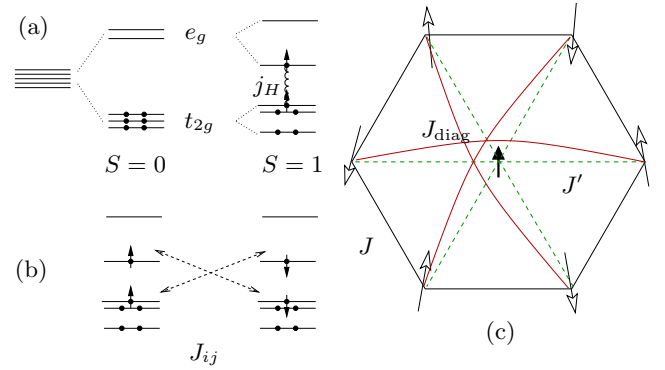


FIG. 1: (Color online) (a) Cubic symmetry for the  $\text{Co}^{3+}$ -ion is removed next to a hole ( $\text{Co}^{4+}$ -ion), this reduces the energy splitting between  $t_{2g}$  and  $e_g$  levels of  $\text{Co}^{3+}$ ; Hund's rule coupling  $j_H$  then stabilizes  $S = 1$  instead of  $S = 0$ . (b) Virtual  $t_{2g}$ - $e_g$  hopping leading to antiferromagnetic coupling  $J_{ij}$  between two  $\text{Co}^{3+}$  ions. (c) Spin structure and interactions within the polaron:  $\text{Co}^{4+}$  with  $s = 1/2$  in the center, induced spin  $S = 1$  on the six adjacent  $\text{Co}^{3+}$ -sites. ( $\text{Co}^{3+}$ -ions further away have  $S = 0$ .) Parameters:  $J$  couples nearest neighbor (n.n.) spins with  $S = 1$  on the ring,  $J_{\text{diag}}$  couples them across the diagonal, both are antiferromagnetic.  $J'$  couples the central  $s = 1/2$  to the ring.

and thereby provide the first quantitative description of the exotic magnetic properties including the negative Curie-Weiss temperature  $\theta$ , the magnitude and temperature dependence of the susceptibility, as well as a small ferromagnetic in-plane coupling mediated by dilute polarons. Further, we discuss the expected impact on magnetic response and predict, apart from the observed spin-waves, additional scattering at specific momenta and energies, which can be verified experimentally.

In  $\text{NaCoO}_2$ , the  $\text{Co}$ - $d$  orbitals are split into energetically lower  $t_{2g}$  and higher  $e_g$  states, and the six electrons of the  $\text{Co}^{3+}$ -ions occupy the  $t_{2g}$  orbitals, leading to a non-magnetic  $t_{2g}^6$  configuration. Consequently,  $\text{NaCoO}_2$  has rather small susceptibility [6]. Removing some of the sodium induces holes and the  $\text{Co}^{4+}$ -sites are found in a  $t_{2g}^5$  configuration with spin  $s = 1/2$ . The few dilute

spins embedded in a non-magnetic background, however, would give orders of magnitude smaller susceptibility at room temperature than observed [3, 11]. The key to the problem is found in the orbital degree of freedom: The  $\text{Co}^{4+}$ -holes removes cubic symmetry at the six surrounding  $\text{Co}^{3+}$ -ions, this splits the  $t_{2g}$ -triplet and the  $e_g$ -doublet (on top of the trigonal splitting induced by the layered crystal structure) and thus reduces the energy gap between the highest  $t_{2g}$ - and the lower  $e_g$ -orbitals, see the schematic representation in Fig. 1(a). The gap actually becomes smaller than Hund's rule splitting, i.e., energy can be gained by transferring one of the electrons from the highest  $t_{2g}$ -level into the lowest  $e_g$ -orbital and forming a triplet with the remaining unpaired electron [13, 14].

The mechanism of polaron formation by holes inducing an energy splitting between orbitals is similar to the orbital-polaron formation considered for lightly doped  $\text{LaMnO}_3$  [15], however, the 90-degree angle of the Co-O-Co bonds causes an important difference: While the spin coupling is ferromagnetic in manganites (leading to a large total spin of the polaron), the coupling in the present case is *antiferromagnetic* [13]. Because of the 90° angle,  $e_g$ - $e_g$ -exchange is suppressed, and the dominant  $t_{2g}$ - $e_g$  process, shown in Fig. 1(b), favors antiferromagnetic alignment of the two ions, as well as an analogous  $t_{2g}$ - $t_{2g}$  hopping. The resulting spin-orbital polaron is depicted in Fig. 1(c). A similar antiferromagnetic exchange  $J_{\text{diag}}$ , induced via virtual longer-range hopping  $t'$ , couples the  $S = 1$ -sites along the diagonals of the polaron and they also couple to the central  $s = 1/2$ . These dressed carriers instead of bare holes are in agreement with ARPES measurement indicating a strongly renormalized quasi-particle band width [16, 17].

The effective spin Hamiltonian resulting from these considerations is given by:

$$H = J \sum_{i=1}^6 \vec{S}_i \vec{S}_{i+1} + J_{\text{diag}} \sum_{i=1}^3 \vec{S}_i \vec{S}_{i+3} + J' \sum_{i=1}^6 \vec{s}_0 \vec{S}_i, \quad (1)$$

where  $S_i, i = 1, \dots, 7, S_7 \equiv S_1$  denote the  $S = 1$  spins in the outside ring and  $s_0$  the  $s = 1/2$  in the center.  $J, J_{\text{diag}}$ , and  $J'$  are the coupling constants: From the orbital structure,  $J \approx 10 - 20 \text{ meV}$ ,  $J_{\text{diag}} \lesssim J$  can be inferred [13]. The coupling  $J'$  of the central  $s = 1/2$  to the outside spins is less clear because ferromagnetic and antiferromagnetic contributions compete, it can *a priori* be positive or negative. As the Hilbert space of this Hamiltonian is only 1458, we easily diagonalize it and compute observables at any temperature.

The susceptibility is particularly interesting:

$$\chi(T) = \langle (S_{\text{tot}}^z)^2 \rangle / T = \sum_l \frac{e^{-\frac{E_l}{k_b T}}}{ZT} \langle E_l | \left( \sum_{i=0}^6 S_i^z \right)^2 | E_l \rangle, \quad (2)$$

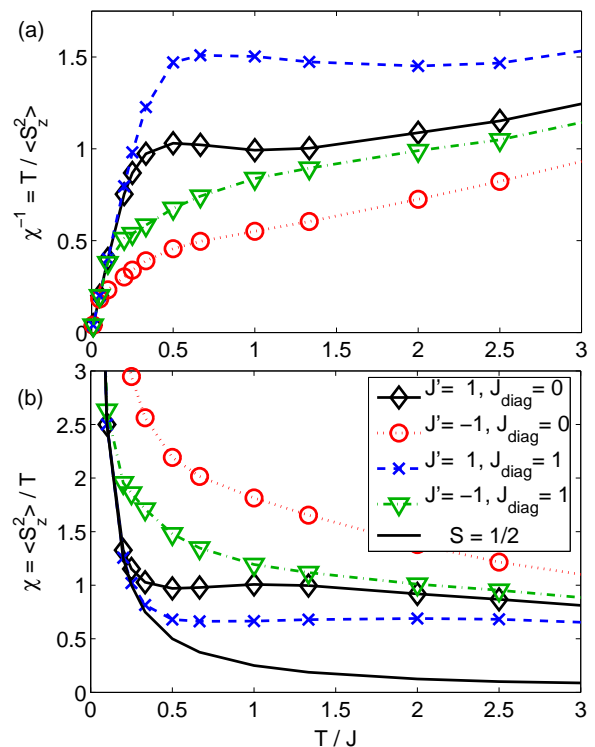


FIG. 2: (Color online) (a) Inverse susceptibility and (b) susceptibility of a polaron, see Fig. 1(c), for some parameter values. For comparison, the susceptibility resulting from a single  $s = 1/2$  spin is included in (b) (solid black line without symbols).

with  $S_{\text{tot}}^z$  the  $z$  component of the total spin and temperature  $T$ .  $E_l$  gives the eigenenergy of state  $|E_l\rangle$ ,  $S_i^z$  the  $z$ -component of the spin at site  $i$ ,  $k_b$  denotes the Boltzmann constant and  $Z = \sum_l e^{-\frac{E_l}{k_b T}}$  the partition function. The inverse susceptibility  $\chi^{-1}$  of a polaron is depicted in Fig. 2(a) for several parameter sets. For all cases, the slope increases for decreasing  $T$ , that is,  $\langle (S_{\text{tot}}^z)^2 \rangle$  becomes smaller. The reason is the freezing of the  $S = 1$  system into a singlet state as the antiferromagnetic bonds become stronger at  $T \ll J$ , which leaves only the net  $s = 1/2$  spin. If the high-temperature part were continued as a straight line, it would cross the  $T$ -axis at  $\theta < 0$ , i.e. give a negative Curie-Weiss temperature.

Figure 2(b) shows the susceptibility of a polaron  $\chi(T)$  depending on temperature for the same parameter sets. We note that comparing the shapes of the curves to experimental susceptibility data [3, 5, 12] points towards  $J' < 0$ . For comparison, we also included the susceptibility  $\chi = 1/4T$  of a single  $s = 1/2$ , which would be obtained, if we had only the  $s = 1/2$  resulting from the  $\text{Co}^{4+}$ -site, i.e., if all  $\text{Co}^{3+}$ -ions would remain in the  $S = 0$  state: For  $T \gtrsim J$ , it is much smaller than the susceptibility of the polaron, regardless of parameter values. Experimentally, the high-temperature values for the susceptibility  $\chi_{\text{exp}}$  for  $0.7 \lesssim x \lesssim 0.9$  range from  $\sim 10^{-4} \text{ emu/mol}$

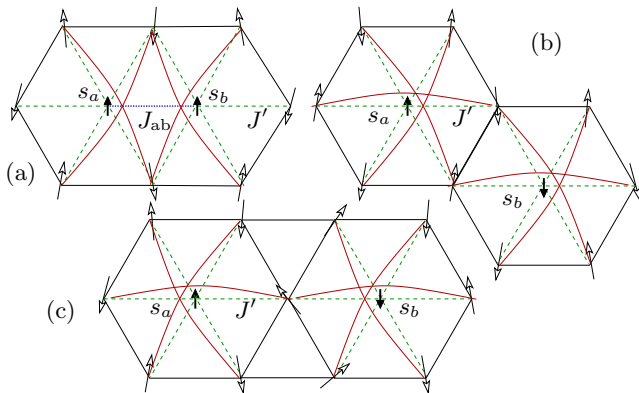


FIG. 3: (Color online) Three possible configurations of interacting polarons.  $J_{ab}$  gives the bare ferromagnetic coupling between  $s_a$  and  $s_b$ , remaining couplings and symbols as Fig. 1(c).

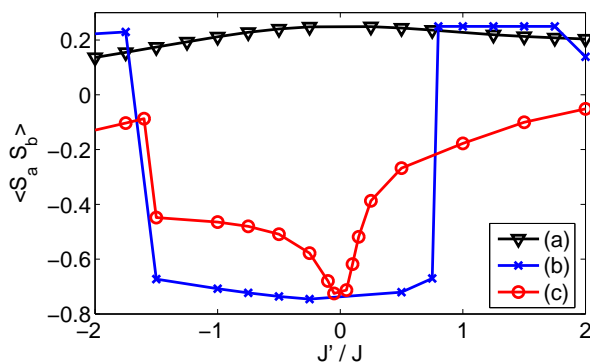


FIG. 4: (Color online) Ground-state spin correlations  $\langle \vec{s}_a \vec{s}_b \rangle$  between the two  $\text{Co}^{4+}$  sites for the interacting-polaron configurations depending on  $J'$ . (a), (b) and (c) indicate the cluster as depicted in Fig. 3.  $J_{\text{diag}} = J$ ,  $J_{ab} = 0$ .

to  $\sim 10^{-3}$ emu/mol [3, 5, 6, 11, 12, 18]. From our high-temperature values for the susceptibility of a single polaron  $\chi_{\text{polaron}} \approx 1/J$ , see Fig. 2(b), the susceptibility per mole is obtained via

$$\chi_{\text{theory}} = \frac{g^2 \mu_B^2 N_A}{J} (1-x) \chi_{\text{polaron}}, \quad (3)$$

with Landé g-factor  $g = 2$ , Bohr magneton  $\mu_B$ , Avogadro's constant  $N_A$  and doping  $x$ . Taking  $J = 20$  meV,  $x = 0.82$ , this corresponds to  $\chi_{\text{theory}} \approx 1.2 \times 10^{-3}$ , in accordance with the value reported for  $\text{Na}_{0.82}\text{CoO}_2$  [12]. Both the shape, see Fig. 2(b) and the absolute values of the susceptibility obtained with the polaron model therefore agree well with experiment.

While we have solved the riddle of the susceptibility, we have still to show how ferromagnetic interactions within the plane can arise and lead to the A-type antiferromagnetism observed below 20K [7, 8]. To this end, we analyze three configurations of interacting polarons depicted in Fig. 3, which will occasionally occur as two mobile polarons come near each other. At first, we examine the

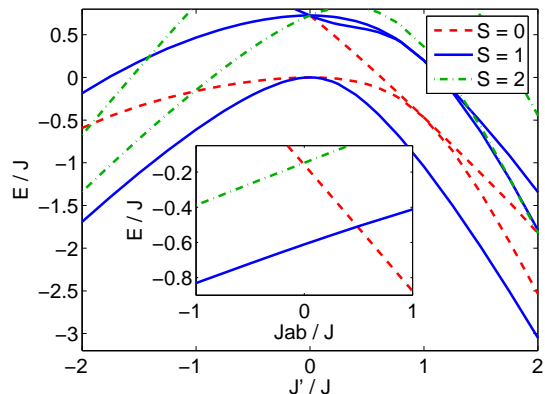


FIG. 5: (Color online) Energies of the lowest states with  $S_{\text{tot}}^z = 0, 1, 2$  for the bi-polaron Fig. 3(a) depending on  $J'$  for  $J_{ab} = 0$  (main panel) and depending on  $J_{ab}$  for  $J' = -J$  (inset).  $J_{\text{diag}} = J$ .

direct coupling  $J_{ab}$  between two  $\text{Co}^{4+}$ -ions situated at n.n. sites as in the bi-polaron Fig. 3(a). Like the coupling between  $\text{Co}^{3+}$ -spins  $J$ , it originates from virtual hopping processes over a 90-degree Co-O-Co path; it is composed of both ferromagnetic and antiferromagnetic terms. With an average hole density  $n = 1/3$  in each  $t_{2g}$  orbital, we can obtain it from Eqs. (5.5.) to (5.7.) of Ref. 13, with  $A \approx B \approx C/2$ . We arrive at  $J_{ab} = -8/9A$ , which is  $\sim -J$ , because  $A$  and  $J$  are of the same scale. The ferromagnetic net interaction is due to a dominance of Hund's-rule coupling over the other terms.

However, it is not obvious that the more complex polarons do not mediate a different and possibly antiferromagnetic interaction and thus turn the net in-plane interaction from ferro- to antiferromagnetic. We therefore solve the complete model given by the clusters in Fig. 3, and as the Hilbert space is here larger, we employ the Lanczos algorithm. From the low-energy eigenstates, we calculate observables like the spin-spin correlation between the two  $\text{Co}^{4+}$ -sites  $\langle \vec{s}_a \vec{s}_b \rangle$ , which we show in Fig. 4 in absence of  $J_{ab}$ . For the bi-polaron Fig. 3(a), we see that the ground state favors ferromagnetic alignment, while it is antiferromagnetic for the two clusters with larger distance between the  $\text{Co}^{4+}$ -ions.

In order to make a statement on the size of the resulting effective exchange, we have to consider the involved energies. For the bi-polaron Fig. 3(a), i.e. for the n.n. case, they are shown in Fig. 5 for different values of the  $z$ -component of the total spin (a good quantum number)  $S_{\text{tot}}^z = 0, 1, 2$ . As expected, the singlet and triplet states are degenerate for  $J' = 0$ , i.e., when the  $\text{Co}^{4+}$  states are not coupled to the  $\text{Co}^{3+}$  system. For  $|J'| > 0$ , the ferromagnetic triplet state has lower energy than the antiferromagnetic singlet state, i.e., the effective interaction via the  $S = 1$ -system strengthens the direct ferromagnetic interaction. The effective interaction is then combined with the direct coupling  $J_{ab}$  and the inset of

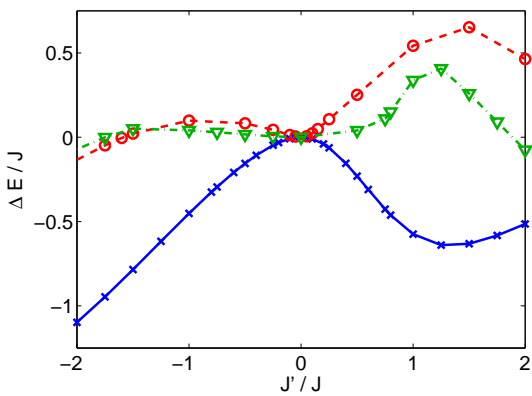


FIG. 6: (Color online) Singlet-triplet gap depending on  $J'$  for all three clusters: crosses for the bi-polaron Fig. 3(a), triangles for Fig. 3(b), and circles for Fig. 3(c).  $J_{\text{diag}} = J$

Fig. 5 shows the energies of the lowest bi-polaron states for  $J' = -J$  depending on  $J_{ab}$ . We see that the energy change is  $\approx J_{ab}\langle s_a s_b \rangle$ , i.e. the two contributions can be simply added  $J_{\text{bipol.}} \approx J_{\text{bipol.}} + J_{ab}$ .

Next, we perform a similar analysis on the two other configurations of edge- or corner-sharing polarons. As can be seen in Fig. 4, we actually find that the ground states have antiferromagnetically coupled  $\text{Co}^{4+}$ . The energy difference between the lowest triplet state and the singlet ground state, which is equivalent to an effective antiferromagnetic next nearest neighbor (n.n.n.) coupling, is depicted in Fig. 6. While it nearly vanishes for  $J' < 0$ , it becomes comparable to the ferromagnetic n.n. exchange  $J_{ab}$  for  $J' > 0$ , especially if one considers that there are twice as many possible n.n.n. interactions as n.n. ones (i.e. 12 instead of 6). Such an effective antiferromagnetic long-range coupling between the polarons should manifest itself as a deviation from a n.n. Heisenberg-like dispersion in spin-wave measurements. While the fact that such a deviation was not observed might result from too small momentum vectors in experiment, it could also indicate that  $J'$  is, in fact, negative, which leads to negligible n.n.n.-coupling, see Fig. 6. The spin-wave dispersion thereby provides a way to experimentally determine the sign of  $J'$ .

For the n.n. coupling and  $|J'| \lesssim J$ , which we believe to be a realistic range based on the susceptibility data, we read off a ferromagnetic exchange  $0 > J_{\text{bipol.}} \gtrsim -0.5J$  (see Fig. 6) in addition to the direct  $J_{ab} \sim -J$ . However, the ferromagnetic coupling is substantially reduced by the fact that only some bonds are covered by bi-polarons. For hole density  $\delta \equiv 1 - x$ , we have  $J_{\text{av}} \simeq (J_{\text{bipol.}} + J_{ab}) \cdot \delta$ . At  $\delta \approx 0.2$  and  $J' = -J$ , this gives an average exchange  $J_{\text{av}} S_i S_j$  with  $J_{\text{av}} \sim -6$  meV, which agrees well with measured values of  $\sim -8$  meV [7, 19] and  $\sim -6$  meV [8].

We have already shown that the internal degrees of freedom of the polaron, i.e. the energy-level structure

of the  $s = 1/2$  coupled to a  $S = 1$  ring with a Haldane gap, are crucial for the high-temperature behavior of the static susceptibility  $\chi$ . They likewise influence the dynamic susceptibility  $\chi''(\vec{q}, \omega)$ , where they lead to a quasi-localized mode [13] in addition to the collective and dispersive spin waves. For its experimental observation, it is crucial to know energy and momentum of this mode. We predict here that its largest weight in momentum space is found at  $\vec{q} = K = (4\pi/3, 0, 0)$ , a little is also obtained for  $\vec{q} = M = (0, 2\pi/\sqrt{3}, 0)$ , but the weight is quickly reduced upon approaching the  $\Gamma$ -point  $(0, 0, 0)$  (details for the structure factor will be given elsewhere). The energy of the lowest peak is found at  $\omega \sim J$  for  $J_{\text{diag}} = J, J' = 0$ , and is lowered by a coupling  $|J'| > 0$  to the central  $s = 1/2$ . In spin-wave experiments, large damping is expected at these energies and momenta because the spin waves strongly scatter on the quasi-localized modes. For ferromagnetic  $J' < 0$ , which has already been noted before to be more plausible based on susceptibility and spin-wave data, damping is expected to start between  $\omega \sim J/2$  and  $\omega \sim J$ , depending on  $J'$ , as actually observed in neutron-scattering experiments [7, 8]. For an antiferromagnetic  $J' > 0$ , the energy of the localized mode is reduced much faster and reaches  $\omega = 0$  for  $J' = J$ . This seems to rule out large antiferromagnetic  $J'$ , because spin-waves are actually clearly measurable at not too large energies [7, 8].

To summarize, we present a coherent and quantitative description of the magnetic properties of  $\text{Na}_x\text{CoO}_2$  at large  $x$ . The concept of spin-orbital polarons could likewise be a key in understanding the unconventional transport properties of cobalt-based materials.

We would like to thank B. Keimer, C. Bernhard, S. Bayrakci and A. T. Boothroyd for useful communications.

- 
- [1] K. Takada *et al.*, Nature (London) **422**, 53 (2003).
  - [2] K. Fujita, T. Mochida, and K. Nakamura, Jpn. J. Appl. Phys. **40**, 4644 (2001).
  - [3] M. Mikami *et al.*, 7383 **42**, Jpn. J. Appl. Phys. (2003).
  - [4] Y. Wang, N. S. Rogado, R. J. Cava, and N. P. Ong, Nature (London) **423**, 425 (2003).
  - [5] M. L. Foo *et al.*, Phys. Rev. Lett. **92**, 247001 (2004).
  - [6] G. Lang *et al.*, Phys. Rev. B **72**, 094404 (2005).
  - [7] S. P. Bayrakci *et al.*, Phys. Rev. Lett. **94**, 157205 (2005).
  - [8] L. M. Helme *et al.*, Phys. Rev. Lett. **94**, 157206 (2005).
  - [9] M. J. Lewis *et al.*, Phys. Rev. B **72**, 014408 (2005).
  - [10] J. L. Gavilano *et al.*, Phys. Rev. B **69**, 100404(R) (2004).
  - [11] T. Motohashi *et al.*, Phys. Rev. B **67**, 064406 (2003).
  - [12] S. P. Bayrakci *et al.*, Phys. Rev. B **69**, 100410(R) (2004).
  - [13] G. Khaliullin, Prog. Theor. Phys. Suppl. **160**, 155 (2005).
  - [14] C. Bernhard *et al.*, Phys. Rev. Lett. **93**, 167003 (2004).
  - [15] R. Kilian and G. Khaliullin, Phys. Rev. B **60**, 13458 (1999).
  - [16] M. Z. Hasan *et al.*, Phys. Rev. Lett. **92**, 246402 (2004).

- [17] H.-B. Yang *et al.*, Phys. Rev. Lett. **92**, 246403 (2004).
- [18] J. Sugiyama *et al.*, Phys. Rev. B **69**, 214423 (2004).
- [19] Note that our definition of  $J$  differs by a factor of 2 from

the convention  $2JS_iS_j$  used in [7].